

Prediction of ILI following the COVID-19 pandemic in China by using a partial differential equation

Xu Zhang(张栩), Yu-Rong Song(宋玉蓉), and Ru-Qi Li(李汝琦)

Citation: Chin. Phys. B, 2024, 33 (**11**): 110201. DOI: 10.1088/1674-1056/ad6f90
Journal homepage: http://cpb.iphy.ac.cn; http://iopscience.iop.org/cpb

What follows is a list of articles you may be interested in

Exact solutions for magnetohydrodynamic nanofluids flow and heat transfer over a permeable axisymmetric radially stretching/shrinking sheet

U. S. Mahabaleshwar, G. P. Vanitha, L. M. Pérez, Emad H. Aly, and I. Pop
Chin. Phys. B, 2024, 33 (**2**): 020204. DOI: 10.1088/1674-1056/ad09c9

MetaPINNs: Predicting soliton and rogue wave of nonlinear PDEs via the improved physics-informed neural networks based on meta-learned optimization

Yanan Guo(郭亚楠), Xiaoqun Cao(曹小群), Junqiang Song(宋君强), and Hongze Leng(冷洪泽)
Chin. Phys. B, 2024, 33 (**2**): 020203. DOI: 10.1088/1674-1056/ad0bf4

Analytical wave solutions of an electronically and biologically important model via two efficient schemes

Qingbo Huang, Asim Zafar, M. Raheel, and Ahmet Bekir
Chin. Phys. B, 2023, 32 (**11**): 110201. DOI: 10.1088/1674-1056/ace61f

Positon and hybrid solutions for the (2+1)-dimensional complex modified Korteweg-de Vries equations

Feng Yuan(袁丰) and Behzad Ghanbari
Chin. Phys. B, 2023, 32 (**4**): 040201. DOI: 10.1088/1674-1056/ac935b

Prediction of epidemics dynamics on networks with partial differential equations: A case study for COVID-19 in China

Ru-Qi Li(李汝琦), Yu-Rong Song(宋玉蓉), and Guo-Ping Jiang(蒋国平)
Chin. Phys. B, 2021, 30 (**12**): 120202. DOI: 10.1088/1674-1056/ac2b16

Prediction of ILI following the COVID-19 pandemic in China by using a partial differential equation

Xu Zhang(张栩)[1], Yu-Rong Song(宋玉蓉)[2,†], and Ru-Qi Li(李汝琦)[1]

[1] *School of Computer Science, Nanjing University of Posts and Telecommunications, Nanjing* 210023, *China*
[2] *College of Automation and College of Artificial Intelligence, Nanjing University of Posts and Telecommunications, Nanjing* 210023, *China*

(Received 15 May 2024; revised manuscript received 12 August 2024; accepted manuscript online 15 August 2024)

The COVID-19 outbreak has significantly disrupted the lives of individuals worldwide. Following the lifting of COVID-19 interventions, there is a heightened risk of future outbreaks from other circulating respiratory infections, such as influenza-like illness (ILI). Accurate prediction models for ILI cases are crucial in enabling governments to implement necessary measures and persuade individuals to adopt personal precautions against the disease. This paper aims to provide a forecasting model for ILI cases with actual cases. We propose a specific model utilizing the partial differential equation (PDE) that will be developed and validated using real-world data obtained from the Chinese National Influenza Center. Our model combines the effects of transboundary spread among regions in China mainland and human activities' impact on ILI transmission dynamics. The simulated results demonstrate that our model achieves excellent predictive performance. Additionally, relevant factors influencing the dissemination are further examined in our analysis. Furthermore, we investigate the effectiveness of travel restrictions on ILI cases. Results can be used to utilize to mitigate the spread of disease.

Keywords: partial differential equations, influenza, SIS model, prediction

PACS: 02.30.Jr, 88.10.gc, 02.60.Cb, 87.23.Kg **DOI:** 10.1088/1674-1056/ad6f90

1. Introduction

Despite four years of global dissemination, COVID-19 continues to pose a significant threat across the majority of countries worldwide. In response, numerous educational institutions, workplaces, and public gathering spaces were temporarily closed as part of comprehensive measures aimed at mitigating transmission of SARS-CoV-2.1.[1–5] These interventions have proven successful in helping countries prevent extensive damage caused by the COVID-19 pandemic.[6–8] Measures such as social distancing, mask-wearing, school closures, restrictions on public gatherings and travel, as well as at-home orders have effectively reduced transmission associated with the pandemic.[9–11] Consequently, these measures have also contributed to a decline in other circulating respiratory infections within respective areas.[12,13] Similar reductions in influenza cases were also observed globally during the pandemic.[14–18] Over four years since its emergence, mortality rates have decreased due to widespread vaccination efforts and diminished virulence among new variants. As a result of these advancements and improvements in control strategies against the spread of COVID-19, many countries eased their respective pandemic prevention policies. On 13 December 2023, China announced the relaxation of the epidemic prevention policy.[16] However, the incidence rate for the COVID-19 pandemic has reached an unprecedented peak while simultaneously raising concerns regarding other circulation respiratory infections such as influenza.

Influenza-like illness (ILI) is a significant source of morbidity and mortality worldwide, which can be attributed to a wide range of respiratory viruses, including influenza viruses, adenoviruses, respiratory syncytial virus (RSV), enteroviruses, human metapneumovirus (HMPV), and parainfluenza viruses. Although some symptoms of COVID-19 and ILI are similar, ILI does not include COVID-19. Researchers are developing novel models to predict the epidemic dynamics associated with other circulation respiratory infections, especially ILI.[19,20] Some researchers characterize viral infections in children with influenza-like illness.[21,22] Some characterize the seasonality of ILI.[20,23] In addition, several researchers focus on epidemic spreading, coevolution epidemics spread, and model of voluntary vaccination on higher-order networks.[24–26]

These models typically focus on the temporal evolution of disease within the population disregarding spatial interventions, despite their significant role in transmission systems.[27] It is necessary to consider that the impact of spatial effects is crucial for studying the spread of influenza following the COVID-19 pandemic. Consequently, several spatially extended models have been proposed to provide a more detailed description of epidemics.[28] For example, Wang *et al.* investigate a spatial SI epidemic model with self- and cross-diffusion.[29] Sun investigates a spatial pattern of an epidemic model with nonlinear incidence rates.[30] Li and Nie developed a non-local delayed reaction-diffusion model of Avian influenza with vaccination and multiple transmission routes in the heterogeneous spatial environment.[31] These partial differential equations models are commonly based on parabolic

†Corresponding author. E-mail: songyr@njupt.edu.cn
© 2024 Chinese Physical Society and IOP Publishing Ltd

reaction-diffusion equations, which propagate instantaneously in space at infinite speeds.[32,33]

To address this limitation, we employ the first-order partial differential equations (PDEs) in our work to construct a spatiotemporal model that allows a more detailed description of the dynamics as a study case for developing this model. There have been plenty of models to describe spread of epidemics. Many models that use ordinary differential equations (ODEs) have been proposed for predicting epidemics. These ODE models can reflect the overall trend of diseases, and focus on the temporal evolution of diseases within the population disregarding spatial interventions, despite their significant role in transmission systems. In addition, many researchers focused on models which may be effective in predicting single-wave outbreaks. However, diseases appear to be under-performing for long-term multi-wave outbreaks. Thus, we construct a spatiotemporal model based on PDEs. By fitting in real time, the time-varying parameters of the PDE model are inferred for prediction, the prediction of our model is long-term accurate. Meanwhile, the proposed model describes human activities on the transmission of ILI and provides a new way for quantifying the effectiveness of the government policies toward controlling ILI.

In this paper, we propose a computational model for describing epidemic spread on network based on the first-order partial differential equations (PDE), which focuses on the spread of ILI after relaxing the control implementation of COVID-19. Meanwhile, we analyze the effect of travel restrictions on the spread and outbreak of ILI.

2. Methods

2.1. Data source

Recent influenza-like illness (ILI) data based on laboratory results have been publicly available on the website of the Chinese National Influenza Center. The data can be accessed and downloaded from https://ivdc.chinacdc.cn/cnic/.

The weekly cases for COVID-19 and ILI are shown in Fig. 1(a), where the blue line represents the cases of ILI and the red line stands for the infection number of COVID-19. The number of ILI cases in the 39th week of 2022 in this figure is unavailable. The infection number of COVID-19 is collected from the website of the Chinese Center for Disease Control and can be downloaded from https://www.chinacdc.cn/. In Fig. 1(a), the lines represent the real data collected from the websites. The infection number of COVID-19 is much higher than that of ILI, which the blue line represents ILI undulate invisible. In this figure, we observe that the resurgences of COVID-19 and ILI have staggered peak timing. The spread of COVID-19 and corresponding measures taken for curb of spread impact the spread of ILI. While in Fig. 1(b), different lines represent the data for different years. The number of cases at several weeks is unavailable. Meanwhile, we observe that the incidence of ILI has been steadily rising coinciding with the gradual easing of restrictions since 2020.

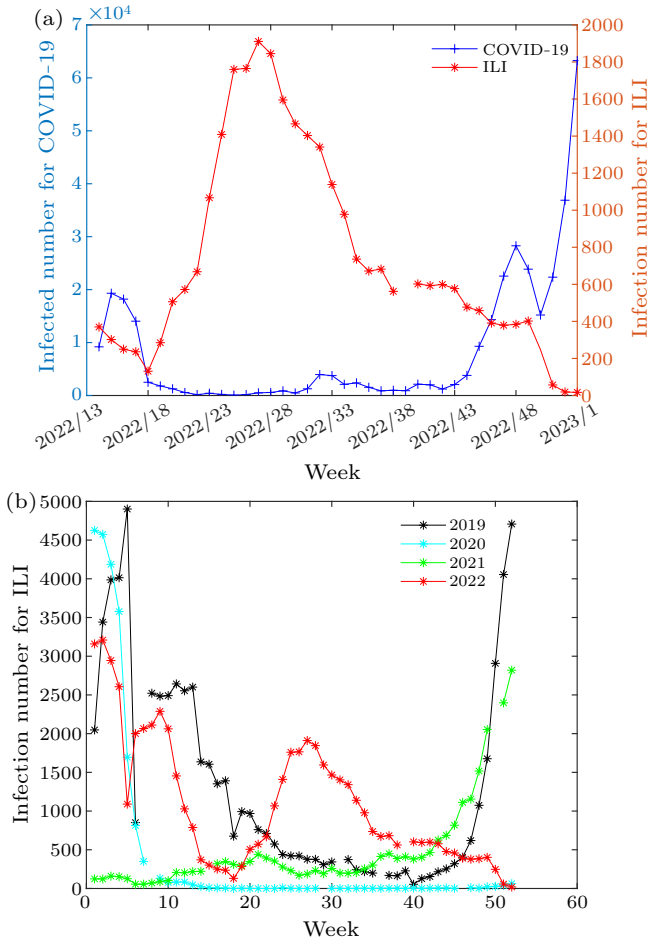


Fig. 1. Weekly incident data for COVID-19 and ILI. (a) Weekly incident data for COVID-19 and ILI from 14th week of 2022 to 1st week of 2023. (b) Weekly incident data for ILI from 1st week of 2019 to 52nd week of 2022.

2.2. Embedding and clusters

The modeling of epidemic spreading has extensively utilized complex networks to represent systems with interacting components. Nodes on the network can represent individual entities or groups of individuals typically villages, cities, provinces, regions, or even countries or locations that are connected.[34,35] Edges on the network can signify transmission events or infectious attempts as well as social relationships facilitating the spread of infection.[36]

Therefore, we consider a spatial network where nodes represent groups of individuals, typically regions. These regions are embedded into Euclidean space and arranged according to their location from region 1 to region N in Fig. 2. Subsequently, we project these N regions onto the x-axis of the Cartesian coordinates with respective locations ranging from 1 to N. Here, we construct a model of epidemics propagating among these regions and the closeness among the several regions.

The changing rate depends on two processes as shown in Fig. 2. (1) Global process: Individuals' commuting and traveling between regions contribute to the spread of disease. (2) Local process: Individuals become infected with infected people in each region, and people may take personal precautions to reduce and mitigate epidemic spread.

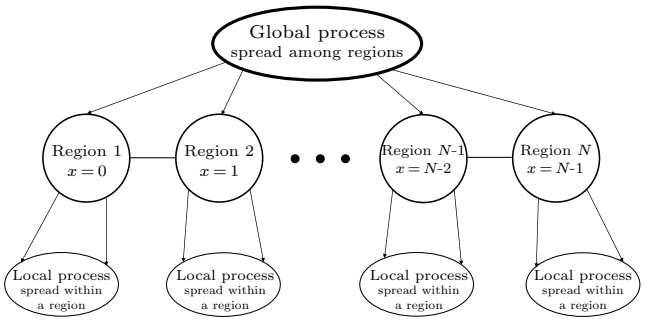


Fig. 2. The N regions are embedding into the x-axis and the two spreading processes.

Let $u(x,t)$ denote the density of the infected individuals at location x and time t, with $x \in [0, N-1]$ for convenience of mathematical description, with $N < \infty$. Here, $\int_a^b u(x,t)\,\mathrm{d}x$ is the density of the infected individuals having the location in the interval $[a,b]$ at time t. Let $U(x,t) = \int_0^x u(y,t)\,\mathrm{d}y$ be the density of the infected individuals having locations less than or equal to x at time t. Let c_x be the individuals moving velocity at location x, in which c_x is constant. The displacement of moving on the x-axis is $c_x h$ in the interval $[t, t+h]$. Let us assume to neglect the dynamics represented by birth and death because of the time scale considered. Let $F(x,t,u)$ denote the function which describes the density of individuals who are infected by infective individuals. The total changing size of the density of the infected individuals is the total density of individuals infected by infective individuals, that is,

$$U(x+c_x h, t+h) - U(x,t) = \int_0^x F(y,t,u)\,\mathrm{d}y. \tag{1}$$

The instantaneous rate of change of the size of the density is

$$\begin{aligned} &\lim_{h\to 0} \frac{U(x+c_x h,t) - U(x,t+h)}{h} \\ &= U_t(x,t) + c_x U_x(x,t) = \int_0^x u_t(y,t)\,\mathrm{d}y + c_x u(x,t). \end{aligned} \tag{2}$$

Diving Eq. (1) by h and then letting $h \to 0$ yield

$$\int_0^x u_t(y,t)\,\mathrm{d}y + c_x u(x,t) = \int_0^x F(y,t,u)\,\mathrm{d}y. \tag{3}$$

Differentiating Eq. (3) with respect to x, we have

$$\frac{\partial u(x,t)}{\partial t} + c_x \frac{\partial u(x,t)}{\partial x} = F(x,t,u). \tag{4}$$

The boundary condition is $u(x,0) = \phi(x)$, which is the initial distribution of the density of the infected individuals.

Thus, we obtain

$$\frac{\partial u(x,t)}{\partial t} + c_x \frac{\partial u(x,t)}{\partial x} = F(x,t,u),$$

$$u(x,0) = \varphi(x), \quad x \geq 0. \tag{5}$$

From the computational perspective, Eq. (5) is computationally efficient which is allowed to compute each location concurrently. If a network contains sufficient clusters, Eq. (5) can be applied to its cluster networks to take advantage of spatiotemporal modeling on networks.

3. PDE model

In this section, we introduce a specific PDE model to accurately describe the dynamics of ILI cases.

3.1. Mathematic model

One of the standard models widely used in epidemic spreading is the SIS model, which assumes that the population can be divided into two classes: the susceptible (S) and the infectious (I). Considering the time scale, we neglect the vital dynamics represented by birth and death. To describe the spatiotemporal dynamics of the population we employ an SIS-type velocity model. It is important to notice that in this model, individuals in class I include asymptomatic cases, who still act as infected and can transmit the disease. Furthermore, we assume that an individual still can be infected even after recovered.

The changing rate of $u(x,t)$ combining the two processes shown in Fig. 2 reads

$$\begin{aligned} \frac{\partial u(x,t)}{\partial t} + c_x \frac{\partial u(x,t)}{\partial x} &= \lambda(x,t)[\rho(x) - u(x,t)] - r(x)u(x,t), \\ u(x,0) &= \phi(x), \quad 0 \leq x \leq N-1. \end{aligned} \tag{6}$$

The parameters of Eq. (1) are listed as follows: (1) c_x describes the transportability of infected individuals at location x. To be simple, we assume that $c_x = c_0 + \mathrm{e}^{-c_1(x-c_2)}$, which is constant. Here c_0, c_1, and c_2 are parameters which need to be determined by the real data. (2) $\rho(x)$ presents the density of population at location x. The total number of individuals is $\int_0^{N-1} \rho(x)\,\mathrm{d}x$. (3) $\lambda(x,t)$ is the infected rate of the collected cases at location x and time t. It represents the spatio-temporal heterogeneity of ILI, which depicts different infection rates in different regions and time. (4) $r(x)$ is the recovered rate of the collected cases at location x, which respects different recovered rates in different regions. To be simple, we assume that $r(x) = r_0 + \mathrm{e}^{-r_1(x-r_2)}$, which is constant. Here r_0, r_1, and r_2 are parameters which need to be determined by the real data.

Initial function $u(x,0) = \phi(x)$ describes the initial states of ILI cases in every region in China mainland, which can be built by historical data of ILI cases.

3.2. Model analysis

We assume

$$\lambda(x,t)=\int_0^{N-1}\beta(x,x')u(x',t)\,\mathrm{d}x', \tag{7}$$

where $\beta(x,x')$ represents the rate of infection from an infective individual at location x with a susceptible at location x', and it depicts different infection rates in different regions.

For this model, the steady state $u(x)$ satisfies the ordinary differential equations corresponding to Eq. (6) with the time derivatives set equal to zero. The steady-state solution reads

$$u(x)=\mathrm{e}^{-\int_0^x\frac{\lambda(y)\rho(y)+\gamma(y)}{c(y)}\mathrm{d}y}\int_0^x\frac{\lambda(z)}{c(z)}\mathrm{e}^{\int_0^z\frac{\lambda(y)\rho(y)+\gamma(y)}{c(y)}\mathrm{d}y}\mathrm{d}z. \tag{8}$$

Substituting the steady-state solution $u(x)$ into the expression for $\lambda(x)$ in Eq. (7) yields

$$\lambda(x)=\int_0^{\infty}\beta(x,x')\,\mathrm{e}^{-\int_0^{x'}\frac{\lambda(y)\rho(y)+\gamma(y)}{c(y)}\mathrm{d}y}\times\left[\int_0^{x'}\frac{\lambda(z)}{c(z)}\mathrm{e}^{\int_0^z\frac{\lambda(y)\rho(y)+\gamma(y)}{c(y)}\mathrm{d}y}\mathrm{d}z\right]\mathrm{d}x'. \tag{9}$$

For simplicity, one possibility here would be separable pair formation, $\beta(x,x')=f(x)g(x')$, thus

$$\lambda(x)=f(x)\int_0^{N-1}g(x')\,\mathrm{e}^{-\int_0^{x'}\frac{\lambda(y)\rho(y)+\gamma(y)}{c(y)}\mathrm{d}y}\times\left[\int_0^{x'}\frac{\lambda(z)}{c(z)}\mathrm{e}^{\int_0^z\frac{\lambda(y)\rho(y)+\gamma(y)}{c(y)}\mathrm{d}y}\mathrm{d}z\right]\mathrm{d}x'. \tag{10}$$

We assume $\lambda(x)=kf(x)$, provided that $kf(x)=f_0+\mathrm{e}^{-f_1(x-f_2)}$, which is constant. Here f_0, f_1, and f_2 are parameters which need to be determined by the real data. Then we obtain

$$1=\int_0^{N-1}g(x')\,\mathrm{e}^{-\int_0^{x'}\frac{kg(y)\rho(y)+\gamma(y)}{c(y)}\mathrm{d}y}\times\left[\int_0^{x'}\frac{f(z)}{c(z)}\mathrm{e}^{\int_0^z\frac{kg(y)\rho(y)+\gamma(y)}{c(y)}\mathrm{d}y}\mathrm{d}z\right]\mathrm{d}x'. \tag{11}$$

Define

$$H(k)=\int_0^{N-1}g(x')\,\mathrm{e}^{-\int_0^{x'}\frac{kg(y)\rho(y)+\gamma(y)}{c(y)}\mathrm{d}y}\times\left[\int_0^{x'}\frac{f(z)}{c(z)}\mathrm{e}^{\int_0^z\frac{kg(y)\rho(y)+\gamma(y)}{c(y)}\mathrm{d}y}\mathrm{d}z\right]\mathrm{d}x'. \tag{12}$$

It is obvious that $H(k)$ is a decreasing function of k. Then $k>0$ provided that $H(0)>1$, and $k<0$ provided that $H(0)<1$. Hence $H(0)=1$ is a threshold for the stability of the infection-free equilibrium. The basic reproduction number R_0 is found by setting $k=0$ in $H(k)$ as follows:

$$R_0=\int_0^{N-1}g(x')\,\mathrm{e}^{-\int_0^{x'}\frac{\gamma(y)}{c(y)}\mathrm{d}y}\left[\int_0^{x'}\frac{f(z)}{c(z)}\mathrm{e}^{\int_0^z\frac{\gamma(y)}{c(y)}\mathrm{d}y}\mathrm{d}z\right]\mathrm{d}x'. \tag{13}$$

Here, R_0 is less than, equal to, or greater than 1, by the k solution of Eq. (11) obtained to be negative, zero, or positive, so that the density of the infected individuals is decaying, constant, or growing, respectively. This expression for the basic reproduction number in the model seems to be new.

4. Prediction of model

Our prediction process is conducted as follows: Firstly, we divide the collected data by the population of each region or the geographic area. Subsequently, we use a three-day training dataset to predict the cases for the following week. For instance, weeks 1–3 are utilized as training data to predict the following week 4, and the accuracy of this prediction is recorded for all regions on week 4.

To fit parameters in the PDE model with actual data, an optimization method is employed. Essentially, this involves solving a multi-parameter inverse problem of hyperbolic equations. We integrate both local and global methods to search for optimal fitting parameters by utilizing the tensor train global optimization 19[37] and the Nelder–Mead simplex method.[38] These methods explore the parameter space for the starting points and perform the local optimization respectively to achieve the goal. It should be noted that the fminsearch function in Matlab comes with the Nelder–Mead simplex method accurately. Once model parameters are determined, we utilize the fourth-order Runge–Kutta method to numerically solve the PDE for one-step forward prediction numerically.

As instance, we give the prediction process for week 4 in detail. Firstly, we interpolate the data of week 1 in constructing the initial function $\phi(x)$ of the PDE model. Then, we use the data of weeks 2 and 3 to train the parameters of the PDE model by the fminsearch function. Finally, we use this PDE model with a new initial function $\phi(x)$ trained by the data of week 3 to predict the results of week 4.

4.1. Prediction of seven regions

As we all know, different geographical environments have different climates, and different regions have different social characteristics. To capture the diverse geographical and social characteristics influencing the spread of ILI, we have categorized China mainland into seven regions: Northeastern China, North China, East China, Central of China, Southern China, Southwestern China, and Northwestern China. Hereafter in this paper, these provincial-level administrative regions will be gathered to as distinct regions representing different aspects related to ILI transmission. Details are as follows: region 1 (Northeastern China) = [Heilongjiang, Jilin, Liaoning]; region 2 (North China) = [Beijing, Tianjin, Shanxi, Hebei, Inner Mongolia]; region 3 (East China) = [Shanghai, Jiangsu, Zhejiang, Anhui, Jiangxi, Shandong, Fujian]; region 4 (Central of China) = [Henan, Hubei, Hunan]; region 5 (Southern China) = [Guangdong, Guangxi, Hainan]; region 6 (Southwestern China) = [Chongqing, Sichuan, Guizhou, Yunnan, Tibet]; region 7 (Northwestern China) = [Shaanxi, Gansu, Qinghai, Ningxia, Xinjiang].

We use the ILI data from the website of the Chinese Center for Disease Control in the province over time. The Chinese Center for Disease Control is compiling the time series data from province and local governments and health departments in an attempt to provide a complete record of the ongoing outbreak. The data can be downloaded from https://www.chinacdc.cn/. If there is missing data, we will use spline interpolation to fill in the data. We compute the weekly new cases of each region by adding the new ILI cases of all provinces belonging to a region. Then, we collect the demographic data from the 2020 population census of China and divide the collected cases by the population of each region to obtain the density of infected individuals in each region. We collect the geographic data from the National Bureau of Statistics and divide the collected cases by the geographic area to obtain the ILI cases per square kilometer in each region.

Figure 3 presents the ILI case predictions for seven regions from the 44th week of 2022 to the 7th week of 2024. The blue lines indicate the predicted ILI cases of the rates of infected individuals and the red lines represent the real data of the rates of infected individuals. The rates of infected individuals are the number of cases divided by the population for each region. Parameters are different in each prediction step, with parameters for the final prediction step (the 7th week of 2024) listed in Table 1. Notably, the PDE-based model has a good prediction.

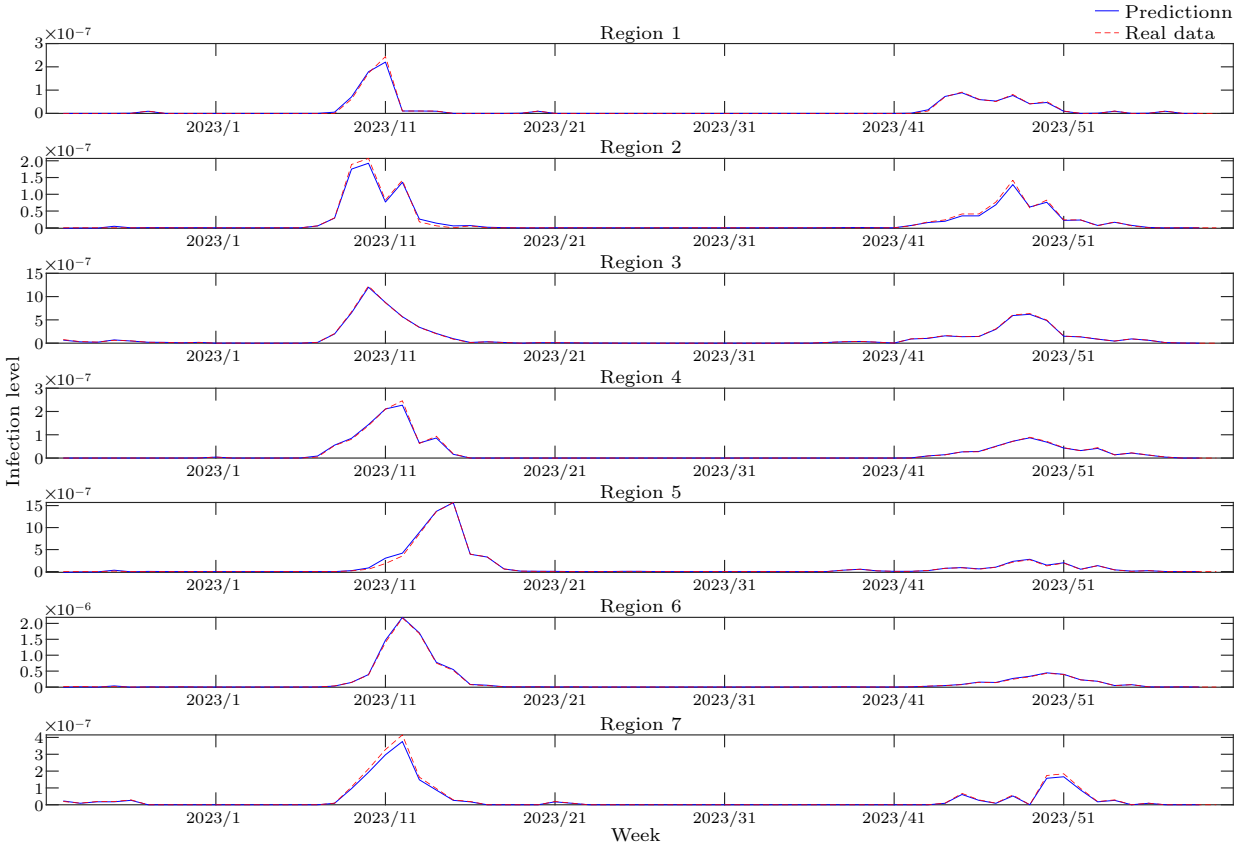


Fig. 3. The weekly cases from 44th week of 2022 to 7th week of 2024. Blue line presents prediction value and red line stands for the actual cases, where the cases are divided by population.

Table 1. The parameters of PDE for the final prediction step.

Parameter	Value	Parameter	Value	Parameter	Value
c_0	1167.601	f_0	1.064483	r_0	1.291496
c_1	0.10039	f_1	1.239087	r_1	1.91243
c_2	0.100049	f_2	0.099778	r_2	2.168168

As is well-known, China lifted the respective implementation of the COVID-19 pandemic on 13 December 2022 (in the 50th week of 2022 in Fig. 3). Around this time, the cases increased significantly while weekly transmission rates for ILI decreased. Simulation results show that compared to the infections of the 50th week of 2023 in Fig. 3, the spread of ILI was fully suppressed after relaxing COVID-19 measures. However, as COVID-19 expanded broadly throughout homes in December 2022, most people focused on stress prevention measures which also proved effective against ILI. The ILI only had a few sporadic cases in the mainland. After a few weeks, as people recovered and made their defenses down completely, there was a rebound in ILI cases. Additionally, the weakened immune system caused by COVID-19 led to reduced

resistance to ILI. Therefore, after relaxing the implemented measures and considering population accumulation during the controlled period the rate of infections experienced a rebound.

As shown in Fig. 3, the magnitude of the ILI outbreak from the 44th week of 2023 to the 1st week of 2024 was significantly larger compared to that observed from the corresponding period in 2022 to the 1st week of 2023. This is attributed to the current widespread prevalence of COVID-19, coupled with heightened public awareness and adherence to preventive measures. Effective individual prevention and control strategies, including stringent personal hygiene practices, mask-wearing, avoidance of crowded areas, and improved indoor ventilation, had also demonstrated a certain inhibitory effect on the transmission of ILI.

As shown in Fig. 3, the spread of ILI reached the peak around the 11th week of 2023. In addition, peak arrival times vary from region to region. In region 5, the peak was reached at the latest in the 14th week of 2023. Climate has played an important role in this phenomenon. Region 5 has a high temperature, which is the region with the highest temperature in the country and experiences an early onset of cases. Region 5 exhibited a delayed peak as case accumulation took longer. In contrast, regions 1 and 7, characterized by colder temperatures, reached their peaks at different times due to variations in population density. Although both the regions had sparse populations, region 7 demonstrated significantly lower average population density compared to that of region 1 resulting in a slower rate of case accumulation. For regions 1 and 3, the temperature in region 1 was much colder than that in region 3. However, due to its vast area and relatively low population density, the time required for case accumulation was prolonged, resulting in a delayed peak.

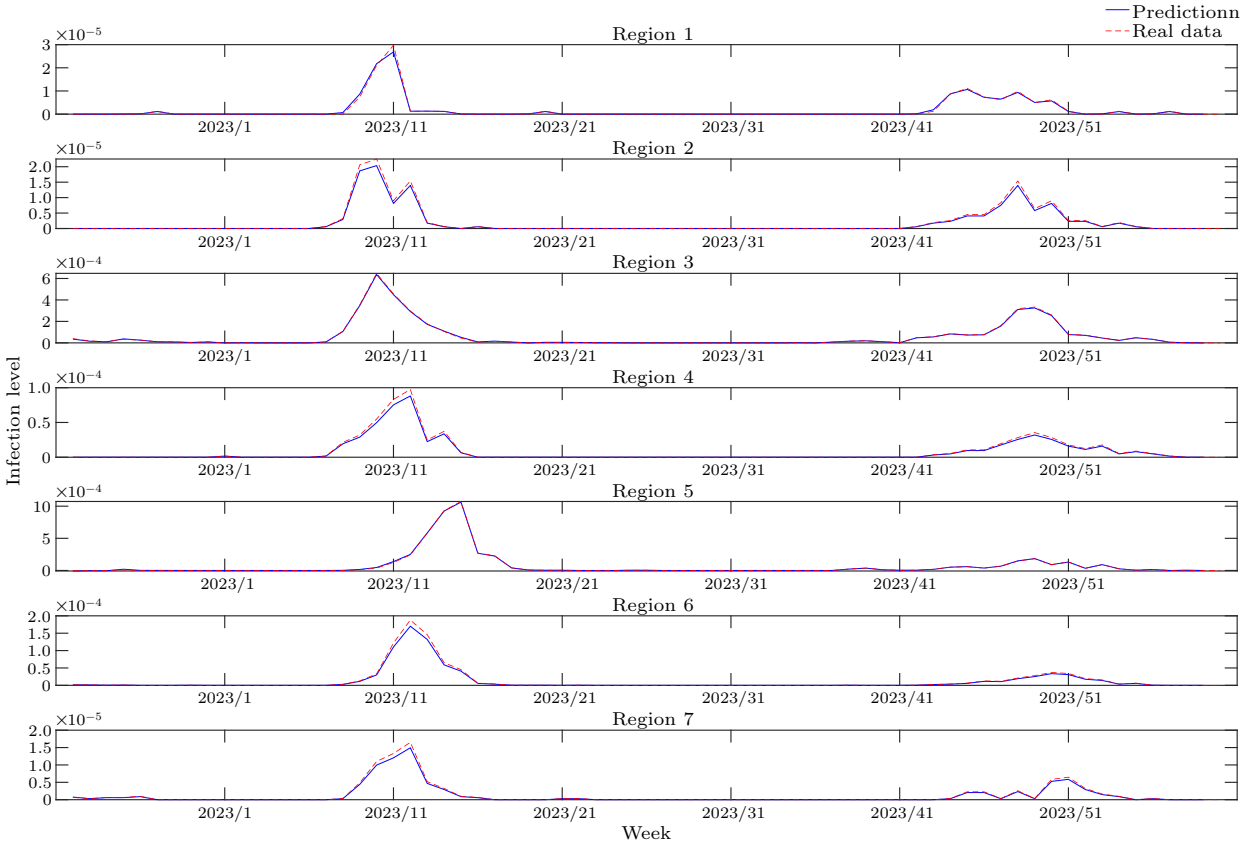


Fig. 4. The weekly cases from 44th week of 2022 to 7th week of 2024. Blue line presents prediction value and red line stands for the actual cases, where the cases are divided by geographic area.

Examining the *y*-axis, it is obvious that region 6 exhibited the highest peak value, followed by region 5. Region 5 had a higher peak value than the other three regions, which can be attributed to its superior population density among all seven regions. Compared with region 6, region 5 surpassed other regions in terms of population, population density, GDP, and economic density despite having a smaller area. The per capita GDP of these two regions is slightly similar. Consequently, to comprehensively assess the impact of population density or geographic area on transmission scale, we divide the cases by the area, i.e., specifically measuring ILI cases per square kilometer, as depicted in Fig. 4. The corresponding parameters for final step (the 7th week of 2024) are listed in Table 2.

According to Fig. 4, it is obvious that the peak value in region 5 was higher than that in region 6. However, population density alone does not account for this difference. Region 1 had a higher population density than region 6, but its peak value was lower than that of region 6. This may be at-

tributed to various factors including urbanization rate, climate conditions, and geographical features such as mountainous areas and plains, which can significantly impact the spread and scale of virus transmission.

Table 2. The parameters of PDE for the final prediction step.

Parameter	Value	Parameter	Value	Parameter	Value
c_0	1199.1	f_0	1.316004	r_0	1.282365
c_1	0.115042	f_1	1.616431	r_1	1.276308
c_2	0.094305	f_2	1.789554	r_2	0.101051

4.2. Prediction in province level

In the above section, we delineated the regions based on geographical and social characteristics and discussed the impact of these two factors on the transmission of the ILI. There are many potential determinants of the spread of the disease, while several potential indicators of economic activity, which include GDP, and per capita GDP, also play a significant role in this regard. In economically prosperous regions, substantial human resources and abundant funding were allocated towards COVID-19 control measures without cost constraints. Consequently, residents with higher incomes possess a greater capacity to safeguard themselves against infection. All these aforementioned factors collectively contributed to subsequent ILI dissemination.

To conduct a comprehensive analysis of these influencing factors, simulations are performed for all 31 provinces and municipalities on the mainland. Subsequently, based on the results obtained, nine provinces and municipalities are selected as depicted in the following. The parameters for final step in Fig. 5 are listed in Table 3. The parameters in Fig. 6 are listed in Table 4.

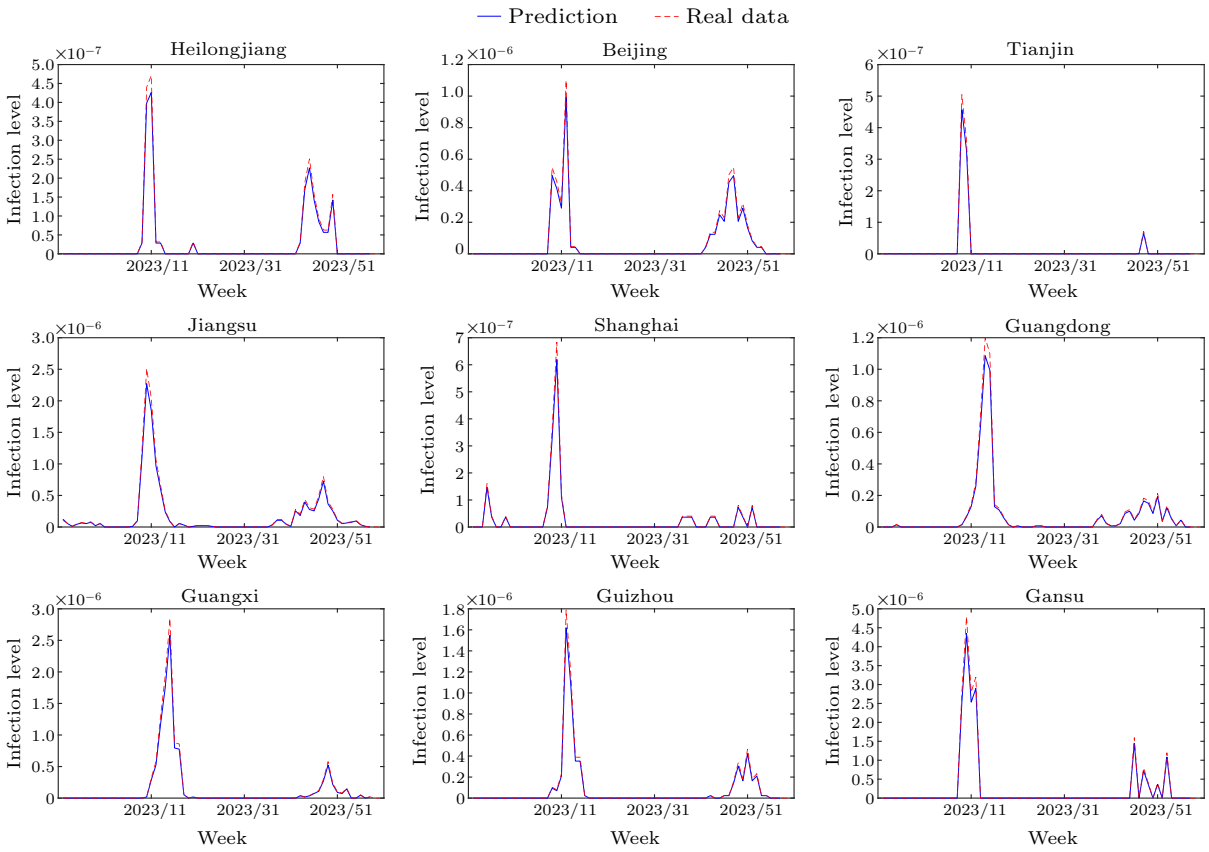


Fig. 5. The weekly cases from 44th week of 2022 to 7th week of 2024 in province level. Blue line presents the prediction value and red line stands for the actual cases, where the cases are divided by population.

Table 3. The parameters of PDE for the final prediction step.

Parameter	Value	Parameter	Value	Parameter	Value
c_0	1055.7	f_0	1.003947	r_0	1.305132
c_1	1.9075	f_1	1.204737	r_1	2.007895
c_2	2.208684	f_2	0.100395	r_2	2.309079

Table 4. The parameters of PDE for the final prediction step.

Parameter	Value	Parameter	Value	Parameter	Value
c_0	1173	f_0	10	r_0	1.3
c_1	0.1	f_1	1.2	r_1	2
c_2	0.1	f_2	0.1	r_2	2.3

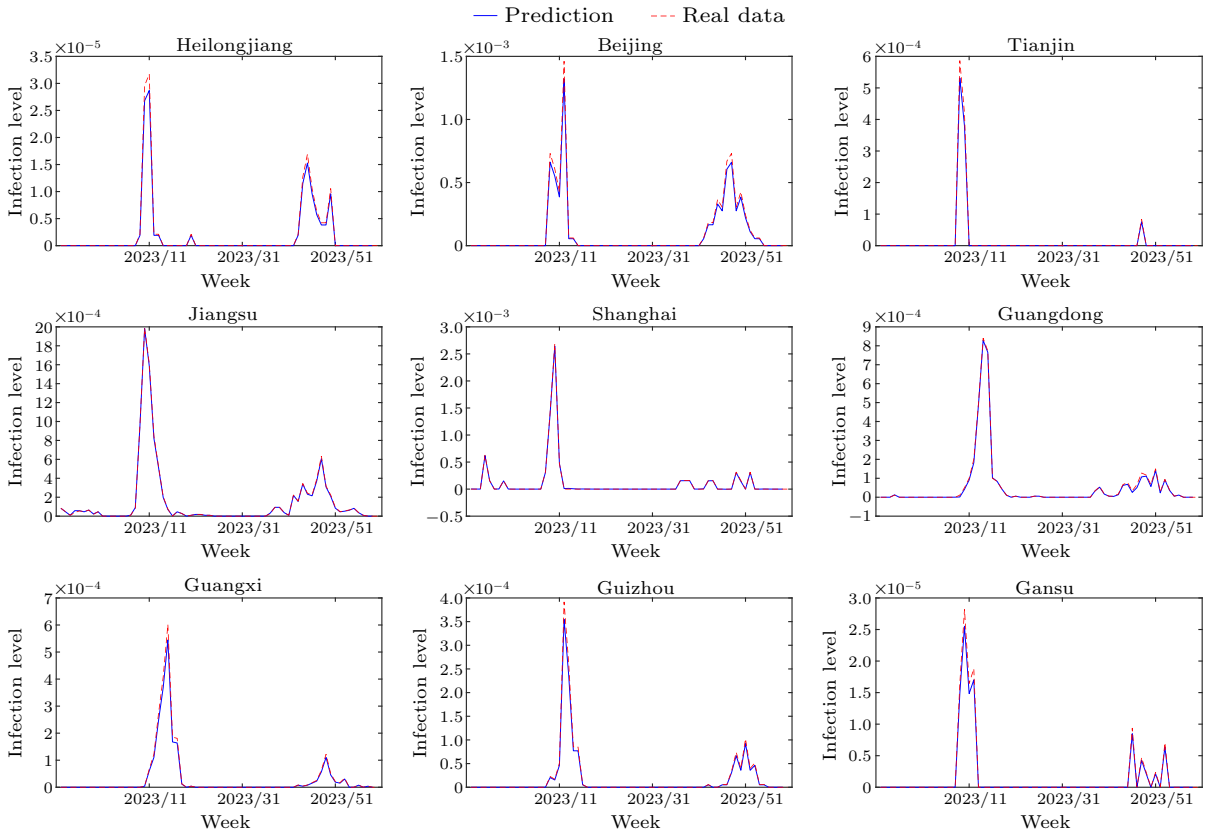


Fig. 6. The weekly cases from 44th week of 2022 to 7th week of 2024 in province level. Blue line represents prediction values and red line stands for the actual cases, where the cases are divided by geographic area.

The ILI case predictions for 31 provinces and municipalities from the 44th week of 2022 to the 7th week of 2024 are simulated and nine of them are shown in Figs. 5 and 6. The blue lines indicate the predicted ILI cases of the rates of infected individuals and the red lines represent the real data of the rates of infected individuals in Fig. 5. The rates of infected individuals are the number of cases divided by the population for each region. In Fig. 6, the blue lines represent the prediction values and the red lines represent the real data of cases. It is obvious that there is a consistent trend between them. Obviously, the PDE-based model has a good prediction.

Compared to Gansu, it is obvious that Heilongjiang exhibits a comparatively colder climate, despite both regions experiencing cold climates. These provinces share similar characteristics such as area size, population density, per capita GDP, and economic density with both being sparsely populated and having the lowest per capita GDP and economic density nationwide. However, there are disparities in terms of population size, urbanization rate, and GDP between the two provinces. Gansu demonstrated a lower urbanization rate while Heilongjiang's urbanization rate fell within the national average range. Additionally, Heilongjiang boasted slightly higher population and GDP figures compared to Gansu. During the first outbreak (around the 10th week of 2023 in Fig. 5), the peaks of both regions were nearly identical in Fig. 5 after relaxing the implemented measures, with Gansu slightly higher than Heilongjiang. The time taken for both regions to reach their respective peaks differed by only one week (the 10th week of 2023 for Gansu and the 9th week of 2023 for Heilongjiang in Fig. 5). In Fig. 6, considering that the y-axis represents the number of infections per square kilometer when comparing similar geographic areas, Heilongjiang exhibits a higher peak compared to Gansu, while maintaining a consistent timing as shown in Fig. 5. This observation may be attributed to factors such as Heilongjiang's larger population, urbanization rate, GDP, and colder temperature conditions. Given that Heilongjiang has more infected individuals due to its larger population size, the proximity of peaks is observed when calculating the probability of infection. However, in terms of cases per square kilometer, Heilongjiang exhibits a higher peak due to its larger number of infected individuals despite similar areas. Hence, population and area aside, GDP and temperature emerge as influential factors for ILI transmission. Notably, temperature plays a crucial role in ILI transmission

within Heilongjiang under comparable GDP conditions.

Compared Guizhou with Guangxi, Guangxi exhibited a comparable climate to Guizhou, even though they had similar geography with karst hills as the main feature. However, there were slight disparities in terms of urbanization rate, population density, per capita GDP, and economic density between the two regions. Specifically, Guangxi demonstrated lower levels of urbanization rate, population density, per capita GDP, and economic density compared to Guizhou. Furthermore, they differed in terms of population size, area coverage, and GDP performance. Notably, Guangxi boasted a larger population than Guizhou along with marginally higher GDP figures; whereas Guizhou possessed a larger land area.

Following the relaxation of implemented measures during the first outbreak period (approximately around the 10th week of 2023 as shown in Fig. 5), Guangxi exhibited a significantly lower peak compared to Guizhou, with their respective peaks occurring at different times (the 14th week of 2023 for Guangxi and the 11th week of 2023 for Guizhou according to Fig. 5). However, as depicted in Fig. 6, Guangxi experienced a higher peak than Guizhou. Despite having more infected individuals and a larger population size which would suggest a lower infection probability leading to decreased intensity, Guangxi exhibited a higher peak when considering average cases per square kilometer due to its smaller geographic area relative to that of the expansive Guizhou province. Henceforth, besides population density and land area factors, GDP emerged as an influential determinant affecting ILI transmission dynamics.

Compared Jiangsu and Guangdong, both the provinces exhibit similar population density and urbanization rates. They possess the highest population density among all provinces, with higher levels of urbanization. However, they differ in terms of population size, area, GDP per capita, and economic density. Guangdong has a larger population and higher GDP compared to Jiangsu, as well as a larger geographical area. On the other hand, Jiangsu boasted a higher per capita GDP and economic density than Guangdong. During the COVID-19 outbreak, both the provinces experienced scattered cases. Following the relaxation of implemented measures (around the 10th week of 2023 in Figs. 5 and 6), Jiangsu witnessed a peak that occurred four weeks later than Guangdong's peak (respectively in the 9th week of 2023 and the 13th week of 2023 in Figs. 5 and 6). This can be attributed to Jiangsu having more people and a smaller geographic area compared to Guangdong. In addition to these factors mentioned above, Guangdong has a higher GDP than Jiangsu while being warmer climatically and all these factors contributed to the greater scale of virus transmission observed in Jiangsu.

Compared to Beijing with Shanghai, both the cities exhibit similar rates of urbanization, GDP, and per capita GDP. They both have higher levels of urbanization, slightly elevated GDP figures, as well as the highest per capita GDP and economic density in China mainland. However, there are differences in terms of area, population density, and economic density. Beijing is marginally larger than Shanghai with a slightly lower population density compared to its counterpart. After the relaxation of implemented measures, during the initial outbreak (around the 10th week of 2023 in Figs. 5 and 6), Beijing experienced a higher peak than Shanghai, reaching its maximum at the 10th week of 2023 while Shanghai peaked at the 9th week of 2023 in Fig. 5. In Fig. 5, Shanghai's peak was higher than that of Beijing. Due to the fact that Beijing has a greater number of infected individuals and a larger population size, the probability of infection reached a higher peak compared to Shanghai. Nevertheless, when considering the average number of infected individuals per square kilometer, Beijing's larger area resulted in a lower peak compared to that observed in Shanghai. Apart from factors such as population and area size, variables such as population density, economic density, and temperature also play significant roles on influencing virus transmission.

Comparing Beijing and Tianjin, the two cities exhibit many similarities in terms of climate, geographical area, population density, and urbanization rate. They have relatively high population densities in China mainland. Both the cities are geographically adjacent and have similar areas. Additionally, they both demonstrate relatively high levels of urbanization. However, there exist differences in terms of population size, GDP, per capita GDP, and economic density. Beijing has a larger population than Tianjin along with significantly higher GDP figures, per capita GDP values as well as economic density levels. After the relaxation of implemented measures during the first outbreak (around the 10th week of 2023 in Figs. 5 and 6), Beijing experienced a higher peak compared to Tianjin's peak, which occurred in the 11th week of 2023 and the 8th week of 2023, respectively (as shown in Fig. 5). It can be inferred that factors such as GDP, per capita GDP, and economic density would contribute to the spread of the virus after accounting for variables like population size and geographical area.

5. Effect of travel restriction method

To mitigate the incidence of ILI cases, we have proposed intervention measures such as implementing travel restrictions during disease outbreaks.

We predict the disease with a decreased value of c_x to indicate the effectiveness of on reducing ILI cases. Here c_x describes the transmission rate of individuals across different regions, which can measure the effect of travel restrictions. Specifically, based on each group of model parameters obtained in the above prediction process, the other parameters remain unchanged in Eq. (6) except multiplying the value of c_x by 50%.

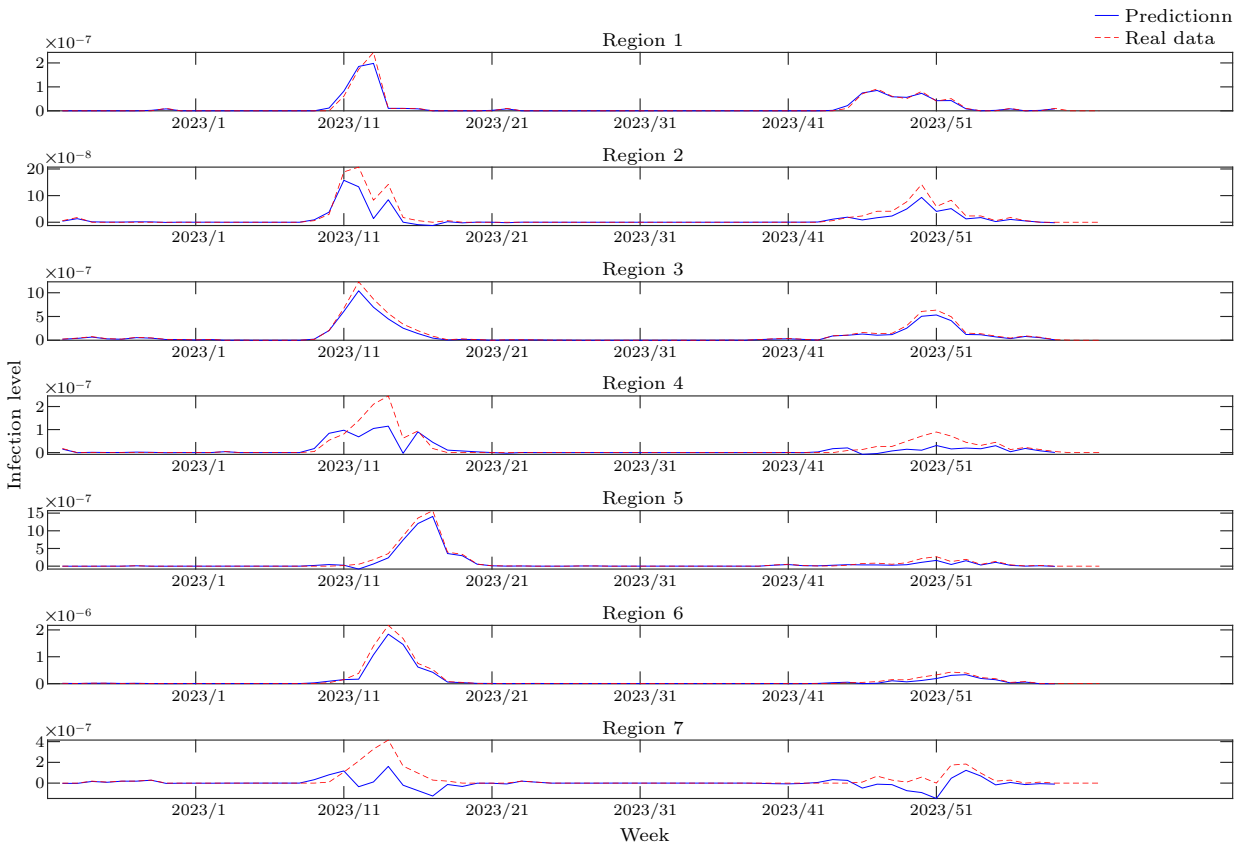


Fig. 7. Preventive measures on the increase of ILI cases from 44th week of 2022 to 4th week of 2024. The red lines stand for the real data for seven regions while blue lines represent the predicted cases under transmission restriction measures.

The ILI cases with the possible intervention for seven regions are illustrated in Fig. 7, where the cases are divided by population. The blue lines depict the predicted cases under measures from the 44th week of 2022 to the 4th week of 2024, while the red lines represent actual data. In comparison to Fig. 3, Fig. 7 demonstrates a decrease in the predicted results when travel restriction is implemented across seven regions. Results reveal that if travel restrictions can be implemented, the highest rates of the spread of ILI will be reduced to percentages ranging from 67.48% to 92.35%, compared to the peak period prior to the implementation of controlled measures. This analysis substantiates the significant impact of precautionary measures on the propagation of the disease. By adaptively taking the travel restriction measures, we can mitigate the resurgence of ILI. Therefore, our results sustain that active travel intervention can effectively inhibit the growth of ILI and curb the wider spread of ILI. Our analysis confirms the positive effects of precaution measures on the spread of ILI.

6. Conclusion and perspectives

In summary, we have proposed a partial differential equation (PDE) model that characterizes various geographical and social factors to predict the incidence of influenza-like illness (ILI) in seven regions in China mainland. Meanwhile, to ensure the accuracy of forecasting, we consider weekly cases of ILI as a reflection of human activities. The results prove that our model can describe the spread of ILI and demonstrate the utility of our model for comprehensive preparedness and control measures against ILI under travel restrictions.

We categorize the 31 provinces, autonomous regions and municipalities, into seven regions, i.e., Northeastern China, North China, East China, Central China, Southern China, Southwestern China, and Northwestern China, which can be naturally projected onto the x-axis of the Cartesian coordinates. This regrouping strategy allows us to avoid computationally intensive calculations while obtaining results with finer granularity to use a computational-heavy PDE model. We choose PDEs instead of ordinary differential equations because partial differential equations can effectively capture the geographical and social behaviors in China mainland in terms of the spread of ILI. Our model for the prediction of regional ILI is based on seven regions, which is the most cost-effective method for predicting ILI across China mainland.

During the COVID-19 control period, community transmission of ILI was suppressed to almost zero. However, after relaxing the control implementation during the COVID-19 pandemic, a significant number of susceptible individuals accumulated ILI cases and reached a new peak due to long-lasting immune damage caused by long COVID-19. Consequently, there is an increased risk of getting influenza-like illness and severe among individuals affected by long COVID-19. Therefore, the quantitative analysis of ILI can provide valuable insights for disease control and prevention strate-

gies aimed at comprehensive preparedness efforts against both COVID-19 and other respiratory illnesses such as ILI. To address these concerns comprehensively, it is important to study how to slow the spread of the disease. The spread of ILI is analyzed by our model, which is evaluated for the coming outbreak after relaxing the control implementation. Taking travel restrictions where the value of c_x reduces to 50%, the peak value of the spread of ILI will be reduced to percentages ranging from 67.48% to 92.35%, compared to the peak period prior to the implementation of controlled measures.

This paper presents a novel partial differentia equation (PDE) model to describe the behavior of the spread of ILI cases between regions, and incorporates human activities for forecasting ILI cases in order to assess the impact of travel restrictions on ILI dynamics. The numerical results demonstrate that our predictive method is of acceptable high accuracy and can effectively forecast the effects of travel restrictions. In conclusion, combining PDE modeling with real data provides insights into the spatiotemporal dynamics of ILI.

However, caution is needed when interpreting these findings. Firstly, the imported cases have not been accounted for in this study, and we only consider infections in China mainland. Second, assume that long COVID-19 has emerged as an endemic respiratory pathogen significantly influencing human behavior patterns. Third, this paper solely presents a qualitative analysis of the influence of geography, economy, and population on the transmission of ILI, without undertaking a quantitative examination. It is important to acknowledge the limitations of our study. Future work will explore alternative approaches such as utilizing a positive piece-wise function to describe $c(x)$ to better capture these complexities.

Data availability statement

The data that support the findings of this study are openly available in Chinese National Influenza Center at https://ivdc.chinacdc.cn/cnic/.

Acknowledgments

This research has been supported by the National Natural Science Foundation of China (Grant No. 62373197) and Postgraduate Research & Practice Innovation Program of Jiangsu Province (Grant No. KYCX18_0892).

References

[1] Bosetti P, Tran Kiem C, Andronico A, Colizza V, Yazdanpanah Y, Fontanet A, Benamouzig D and Cauchemez S 2022 *BMC Med.* **20** 33
[2] Zhang Y, Tao Y, Shyu M, Perry L, Warde P, Messinger D and Song C 2022 *Sci. Rep.* **12** 3044
[3] Huang Y, Shi H, Forgacs D and Ross T 2024 *Vaccine* **42** 1184
[4] Zhu Y, Shen R, Dong H and Wang W 2024 *Chin. Phys. B* **33** 058301
[5] Davies N, Kucharski A, Eggo R, Gimma A and Liu Y 2020 *Lancet Public Health* **5** e375
[6] Li Y, Campbell H, Kulkarni D, Harpur A, Nundy M, Wang X and Nair H 2021 *Lancet Infect. Dis.* **21** 193
[7] Kim J, Roh Y, Ahn J, Kim M, Huh K, Jung J and Kang J 2021 *Int. J. Infect. Dis.* **110** 29
[8] Huang Q, Wood T, Jelley L, Jennings T, Jefferies S, Daniells K, Nesdale A, Dowell T, Turner N, Campbell-Stokes P, *et al.* 2021 *Nat. Commun.* **12** 1001
[9] Feng L, Zhang T, Wang Q, Xie Y, Peng Z, Zheng J, Qin Y, Zhang M, Lai S, Wang D, Feng Z, Li Z and Gao G 2021 *Nat. Commun.* **12** 3249
[10] Yang X, Jiang H, Kang Y, *et al.* 2022 *Chin. Phys. B* **31** 078901
[11] Wang X and Wang L 2022 *Chin. Phys. B* **31** 080204
[12] Li R, Song Y and Jiang G 2021 *Chin. Phys. B* **30** 120202
[13] Liang J, Lin Z, Wang Y, *et al.* 2024 *Front. Cell. Infect. Microbiol.* **14** 1347710
[14] Zhang N, Jia W, Lei H, Wang P, Zhao P Y, Guo Y, *et al.* 2020 *Clin. Infect. Dis.* **73** e1142
[15] Flaxman S, Mishra S, Gandy A, Unwin H, Mellan T, Coupland H, Whittaker C, Zhu H, Berah T and Eaton J 2020 *Nature* **584** 257
[16] Lai S, Ruktanonchai N, Zhou L, Prosper O, Luo W, Floyd J, Wesolowski A, Santillana M, Zhang C, Du X, Yu H and Tatem A 2020 *Nature* **585** 410
[17] Cowling B, Ali S, Ng T, *et al.* 2020 *Lancet Public Health* **5** e279
[18] Xiao J, Dai J, Hu J, *et al.* 2021 *Lancet Reg. Health West Pac.* **17** 100282
[19] Ursinus J, Vrijmoeth H, Harms M, Tulen A, Knoop H, Gauw S, Zomer T, *et al.* 2021 *Lancet Reg. Health Eur.* **6** 100142
[20] Cheng W, Zhou H, Ye Y, Chen Y, Jing F, Cao Z, Zeng D and Zhang Q 2023 *Chaos* **33** 013124
[21] Chao S, Wang Y, Wu B, *et al.* 2024 *Front. Cell. Infect. Microbiol.* **13** 1351814
[22] Oguz M and Senel S 2024 *Human Vaccines & Immunotherapeutics* **20** 2350090
[23] Chen H and Xiao M 2024 *BMC Infect. Dis.* **24** 432
[24] Nie Y, Su S, Lin T, *et al.* 2023 *Commun. Nonlinear Sci. Numer. Simulat.* **127** 107594
[25] Nie Y, Zhong X, Wu T, *et al.* 2022 *Journal of King Saud University -Computer and Information Sciences* **34** 2871
[26] Wang W, Nie Y, Li W, *et al.* 2024 *Phys. Rep.* **1056** 1
[27] Riley S, Eames K, Isham V, Mollison D and Trapman P 2015 *Epidemics* **10** 68
[28] Murray J D 2002 *Photosynthetica* **40** 414
[29] Wang Y, Wang J and Zhang L 2010 *Appl. Math. Comput.* **217** 1965
[30] Sun G 2012 *Nonlinear Dyn.* **69** 1097
[31] Li J and Nie L 2024 *Qual. Theory Dyn. Syst.* **23** 198
[32] Wang Y, Xu K, Kang Y, Wang H, Wang F and Avram A 2020 *Int. J. Environ. Res. Public Health* **17** 678
[33] Wang H and Yamamoto N 2020 *Math. Biosci. Eng.* **17** 4891
[34] Pellis L, Ball F, Bansal S, Eames K, House T, Isham V and Trapman P 2015 *Epidemics* **10** 58
[35] Balcan D, Colizza V, Goncalves B, *et al.* 2009 *Proc. Natl. Acade. Sci. USA* **106** 21484
[36] Lions P and Toscani G 1997 *Revista Matemática Iberoamericana* **13** 473
[37] Oseledets I V 2011 *SIAM J. Sci. Comput.* **33** 2295
[38] Lagarias J C, Reeds J A, Wright M H and Wright P E 1998 *SIAM J. Optim.* **9** 112